Journal of Materials Chemistry B

Accepted Manuscript

ROYAL SOCIETY OF CHEMISTRY

www.rsc.org/materialsB

Effects of functional groups on structure, physicochemical and biological properties of mesoporous bioactive glass scaffolds

Shichang Zhao,‡[a] Jianhua Zhang,‡[bc] Min Zhu,[c] Yadong Zhang,[a] Zhongtang Liu,[d] Yanyu Ma,[c] Yufang Zhu*[c] and Changqing Zhang*[a]

[a] Department of Orthopedics, Shanghai Sixth People's Hospital, Shanghai Jiao Tong University, 600 Yishan Road, Shanghai 200233, People's Republic of China.

[b] School of Medical Instrument and Food Engineering, University of Shanghai for Science and Technology, 516 Jungong Road, Shanghai 200093, People's Republic of China.

[c] School of Materials Science and Engineering, University of Shanghai for Science and Technology, 516 Jungong Road, Shanghai, 200093, People's Republic of China.

[d] Department of Orthopedics, Changhai Hospital, Second Military Medical University, 174 Changhai Road Shanghai 200433, People's Republic of China.

*Corresponding authors:

Prof. Changqing Zhang: Tel: +86 21 64369181; Email: zhangcq@sjtu.edu.cn

Prof. Yufang Zhu: Tel: +86-21-55271663; Email: zjf2412@163.com

‡ The first two authors contributed equally to this work.

The authors declare no competing financial interest.

Abstract: Functionalization of biomaterials with specific functional groups is one of the most straightforward strategies to induce specific cell responses to biomaterials. In this study, thiol (SH) and amino (NH_2) functional groups have been successfully modified on the surfaces of mesoporous bioactive glass (MBG) scaffolds to form thiol-functionalized MBG (SH-MBG) and amino-functionalized MBG (NH_2-MBG) scaffolds by a post-grafting technique. The effects of functional groups on structure, physicochemical and biological properties of MBG scaffolds were systematically investigated. The results showed that the functionalization of MBG scaffolds did not change their structures, and the SH-MBG and NH_2-MBG scaffolds still had hierarchical pore architecture (macropore of 300-500 μm and mesopore of 3.5-4 nm) and high porosity (84-86%), similar to the MBG scaffolds. Furthermore, the SH-MBG and NH_2-MBG scaffolds possessed similar apatite mineralization ability and biocompatibility compared to the MBG scaffolds. Importantly, the SH-MBG and NH_2-MBG scaffolds significantly stimulated adhesion, proliferation and differentiation of human bone marrow-derived mesenchymal stem cells (hBMSCs). Therefore, functionalization of MBG scaffolds with SH and NH_2 functional groups would be a viable way to tailor the surface characteristics for stimulating biological responses of hBMSCs, and the functionalized MBG scaffolds would be a promising bioactive material for bone tissue engineering applications.

1 Introduction

Currently, tissue engineering, the goal of which is the replacement and repair of traumatized, damaged, or missing body tissues with biologically compatible biomaterials, mesenchymal stem/progenitor cells and growth factors, has been paid more and more attention.[1] The biomaterials for tissue engineering must be biodegradable, biocompatible and should be designed to meet both nutritional and biological needs for specific cell behavior involved in new tissue formation. Stem cells are an attractive cell source for tissue engineering and regenerative medicine because they exhibit the capacity to self-renew without loss of their multi-potency and when presented with specific signals can be driven to differentiate down multiple lineages.[2] Bone marrow-derived mesenchymal stem cells (BMSCs) are a potentially valuable cell source for the engineering of damaged or lost connective tissues due to their ability to differentiate into the cells that ultimately generate these tissues, such as adipocytes, chondrocytes, myoblasts and osteoblasts, in the presence of defined environmental factors. However, the development of useful biomaterials for bone tissue engineering is limited due to an incomplete understanding of the specific interface interaction between biomaterials and biological systems. Surface microenvironment characteristics of biomaterials, such as surface energy, chemistry, topography and hydrophobicity, are important factors that influencing the adsorption of various bioactive molecules, hence governing the initial cellular events on the cell-material interface and regulating a wide variety of biological functions, including cell growth, migration, differentiation and synthesis of extracellular matrices

(ECMs).[3, 4] Several studies have suggested that alterations to one or more of these cellular responses at early stages may ultimately result in downstream effects on phenotype-specific gene expression and functional differentiation.[5-8] Therefore, developing biomaterials with the capability to instruct stem cells and control their behavior has a profound effect on the field of bone tissue engineering and will enhance the efficiency of many conceptual and actual tissue-engineered constructs.[9]

Recently, surface modification on biomaterials with chemical groups has been used to develop the controlled drug adsorption and delivery systems.[10-12] Also, surface modification on biomaterials could enhance the growth of hydroxyapatite (HA) on the surface of biomaterials and formation of fibronectin and vitronectin networks, which act as an excellent cell support to maintain desirable cell-substrate interactions, to provide favorable conditions for cell proliferation and to stimulate the osteogenic differentiation.[12-14] The local sustained drug release capability and the improved bioactive behavior of these biomaterials makes them suitable for bone regeneration.[12] Cui et al. investigated HA nucleation and growth on the electrospun poly(DL-lactide) (PDLLA) fibers functionalized with carboxyl (COOH), hydroxyl (OH) and amino (NH_2) groups and their combinations, and the results showed that higher densities of COOH groups, combination of OH and COOH groups with the ratio of 3/7, and combination of NH_2, OH and COOH groups with the ratio of 2/3/5 were favorable for HA nucleation and growth.[13] Toworfea et al. investigated the calcium phosphate deposition through grafting NH_2, COOH and OH-terminal silanes on a fresh silicon oxide surface, and the enhancement of HA nucleation and growth was determined to

be more significant on the hydroxylated (OH) surface.[14] Ahmed El-Fiqi et al. demonstrated that the incorporation of surface-aminated MBG into collagen hydrogels could significantly improve the physicochemical and mechanical properties of collagen hydrogel, leading to a favorable environment for stem cell culture for bone tissue engineering applications.[15] More importantly, Curran et al. produced a range of clean glass with silane-modified surfaces, such as methyl (CH_3), SH, NH_2, OH and COOH, and cultured them in contact with MSCs. The results showed that the CH_3-modified surfaces maintained the MSCs phenotype; the NH_2 and SH-modified surfaces promoted and maintained osteogenesis both in the presence and absence of biological stimuli; the OH and COOH-modified surfaces promoted and maintained chondrogenesis under both basal and chondrogenic stimulated conditions, but did not support osteogenesis.[16] Phillips et al. also showed that self-assembled monolayers (SAMs) of alkanethiols on gold functionalized with different functional groups (CH_3, OH, COOH and NH_2) had different effect on the pattern of fibronectin adsorption, which in turn modulates the osteogenic differentiation of MSCs.[17] Interestingly, the NH_2-SAMs promoted the strongest induction of MSC differentiation along the osteoblastic lineage. Therefore, cell proliferation and differentiation driven by the functionalization of biomaterial surfaces with specific functional groups without the addition of biological stimuli (growth factors, cytokines and other serum proteins) would be a more attractive proposition in terms of implanting tissue-engineered constructs into a host that could elicit a specific cellular response.

Mesoporous bioactive glass (MBG) has been synthesized and proved to exhibit

excellent apatite formation and drug delivery ability compared to conventional BG, because MBG has high specific surface area, large pore volume and mesoporous structure. Therefore, there has been a growing interest in MBG as a bioactive material for bone regeneration.[18, 19] To date, many efforts have been made to fabricate 3D interconnected porous MBG scaffolds, which are beneficial for cell migration, nutrient delivery, vascularization and eventually bone ingrowth.[20, 21] Nevertheless, the surface of MBGs is covered by silanol groups, which is possible to enhance cell responses to MBG materials through surface functionalization with specific functional groups.

To the best of our knowledge, no reports can be found on the study of hBMSCs responses to MBG scaffolds functionalized with different chemical groups. In this work, MBG scaffolds functionalized with SH and NH_2 functional groups were successfully synthesized by evaporation-induced self-assembly process and post-grafting technique. Furthermore, physicochemical properties of these prepared MBG scaffolds were characterized, and adhesion, proliferation and differentiation of hBMSCs cultured on the functionalized MBG scaffolds were systematically investigated.

2 Materials and methods

2.1. Materials.

Nonionic block copolymer $EO_{20}PO_{70}EO_{20}$ (P123, Mw = 5800) was purchased from BASF. Hydrochloric acid (HCl, ≥36%), tetraethyl orthosilicate (TEOS, 98%), triethyl

phosphate (TEP, 99.8%), ethanol (99.7%) and calcium nitrate ($Ca(NO_3)_2•4H_2O$, 99%) were purchased from Sinopharm Chemical Reagent Co. Ltd. 3-mercaptopropyltrimethoxysilane (MPTES, ≥95%) was purchased from Aladdin Chemistry Co. Ltd. 3-aminopropyltriethoxysilane (APTES, ≥98%) was purchased from Sigma-aldrich Co. All chemicals were used without further purification.

2.2. Preparation and surface functionalization of MBG scaffolds.

MBG scaffolds were prepared using co-templates of nonionic block polymer P123 and polyurethane sponges. P123 was used to produce mesopores and polyurethane sponges were used to create macropores according to our previously reported method.[22] In a typical synthesis process of MBG scaffolds, 4.0 g of P123, 6.7 g of TEOS, 1.4 g of $Ca(NO_3)_2•4H_2O$, 0.73 g of TEP and 1.0 g of 0.5 M HCl were dissolved in 60 g of anhydrous ethanol and stirred at room temperature for 24 h. Afterward, the polyurethane sponges (20 ppi) were cleaned and completely immersed in this solution for 10 min. Then they were transferred to a Petri dish and squeezed out the excess sol, then transferred to a Petri dish and allowed to evaporate at room temperature for 12 h, the same procedure was repeated 8 times. When the samples were completely dry, they were calcined at 700 ^{o}C (ramp of 2 ^{o}C/min) for 8 h to obtain the final MBG scaffolds (Ca/P/Si = 15/5/80, molar ratio).

The MBG scaffolds were surface-functionalized with SH or NH_2 groups through a post-synthesis procedure using MPTES and APTES silanes, respectively. Typically, 500 mg of MBG scaffolds was immersed in 100 ml anhydrous ethanol, 1.5 ml of MPTES or APTES was then added into the solution, the mixture was stirred at room

temperature for 48 h. The supernatant solution was discarded and the scaffolds washed with anhydrous ethanol for 3 times. Finally, the functionalized scaffolds were dried at 60 ^{o}C in vacuum oven for 24 h. The bare, SH and NH_2 functionalized MBG scaffolds were named as MBG, SH-MBG and NH_2-MBG scaffolds, respectively.

2.3. Characterization of the functionalized MBG scaffolds.

The wide-angle XRD patterns were obtained on a Bruker D8 advance. Scanning electron microscopy (SEM) was carried out with a FEI Quanta 450 field emission scanning electron microscope. Transmission electron microscopy (TEM) was performed with a JEM-2010 electron microscope operated at an acceleration voltage of 200 kV. N_2 adsorption–desorption isotherms were obtained on a Micromeritics Tristar 3020 at -196 ^{o}C under continuous adsorption conditions. Brunauer-Emmett-Tellwe (BET) and Barrett-Joyner-Halenda (BJH) methods were used to determine the surface area and pore size distribution. Fourier transform infrared (FTIR) spectra were obtained on a Perkin–Elmer SPE CTRUM 100 spectrometer. Zeta potential measurements were performed on a Malvern zeta sizer Nano-ZS90. Thermo gravimetric (TG) analysis was carried out on a Perkin–Elmer Diamond thermobalance between 50 ^{o}C and 800 ^{o}C under a 20 ml/min N_2 flow and at a heating rate of 10 ^{o}C/min.

The porosity of the functionalized MBG scaffolds was measured using Archimedes' principle. Anhydrous ethanol was used as liquid medium. The porosity (P) was calculated according to the following formulation: $P=(W_{sat}-W_{dry})/(W_{sat}-W_{sus})\times100\%$, where W_{dry} is the dry weight of functionalized MBG scaffolds, W_{sus} is the weight of

functionalized MBG scaffolds suspended in anhydrous ethanol and W_{sat} is the weight of functionalized MBG scaffolds saturated with anhydrous ethanol.

The compressive strength of functionalized MBG scaffolds (6×6×6 mm^3) was tested using a Zwick static materials testing machine (5 KN) at a cross-head speed of 0.5 mm min^{-1}. Five samples were used for replicates of this experiment.

2.4. Ion dissolution and apatite formation of the functionalized MBG scaffolds in simulated body fluids (SBF).

To investigate the ion dissolution from functionalized MBG scaffolds, SBF with ion concentrations similar to those in human blood plasma was prepared according to the method described by Kokubo.[23] The functionalized MBG scaffolds were soaked in SBF at 37 ^oC for 3 and 7 days, at 200 ml/g of solution volume to scaffold mass, in accordance with our previous report.[21] After soaking, all the testing scaffolds were collected from SBF solution, rinsed with ethanol and then dried at 37 ^oC. The apatite formation on the surfaces of the functionalized MBG scaffolds was confirmed by SEM, energy-dispersive X-ray spectroscopy (EDS) and XRD analysis. The concentrations of Si, Ca and P ions in SBF solution at predetermined time intervals were determined by inductively coupled plasma optical emission spectroscopy (ICP-OES, Perkin Elmer Optima7000DV). Three samples were used for replicate experiments.

2.5. Cell viability, attachment and proliferation on the functionalized MBG scaffolds.

Primary human bone marrow-derived mesenchymal stem cells (hBMSCs) were

isolated as previously described.[24] The use of human samples was approved by the ethical committee of Sixth People's Hospital, Shanghai Jiao Tong University School of Medicine. In brief, bone marrow (approximately 7 mL) was carefully collected into polypropylene tubes containing preservative-free heparin (1000 U/mL). Then, the marrow was suspended in Dulbecco's Modified Eagle's Medium (DMEM) containing 4.5 g/L glucose (GIBCO, Invitrogen Pty Ltd., Australia), supplemented with 10% fetal bovine serum (FBS), and antibiotics (penicillin G 100 U/mL; and streptomycin 0.1 mg/mL). The cells were plated into dishes and incubated at 37 ^{o}C in a humidified atmosphere with 5% CO_2. Non-adherent cells were removed by changing the culture medium after 5 days of incubation. After 10 days of primary culture, the cells were detached and serially subcultured in 25 cm^2 flasks. The medium was changed every 2-3 days. Cells were detached with 0.25% trypsin, 0.1% EDTA and passaged at 80% confluence. The cells of 4-10th passage were used in the experiments.

The activity of lactate dehydrogenase (LDH) in the culture media released by the cells cultured on the scaffolds was used as an index of cytotoxicity. Briefly, hBMSCs were cultured on the MBG, SH-MBG and NH_2-MBG scaffolds at an initial density of 10^4 cells/scaffold for 3 days, then the culture medium was collected and centrifuged, and the LDH activity in the supernatant was determined by a spectrophotometric microplate reader (Bio-Rad 680, USA) measured at 490nm absorbance according to the manufacturer's instruction (Beyotime).

In order to assess cell adhesion and details of cell/biomaterial interaction, 1×10^5 hBMSCs were cultured on the scaffolds in 24-well culture plate. The cells were then

incubated in DMEM (GIBCO, Invitrogen Pty Ltd., Australia) culture medium supplemented with 10% fetal calf serum (FCS; InVitro Technology, Australia) in humidified culture conditions. After 7 days, the samples were removed from the culture wells, rinsed with PBS, fixed with 2.5% glutaraldehyde in PBS for 1 h. The fixative was removed by washing with buffer containing 4% (w/v) sucrose in PBS and post fixed in 1% osmium tetroxide in PBS followed by sequential dehydration in graded ethanol (50%, 70%, 90%, 95%, 100%) and hexamethyldisilizane (HMDS). The specimens were coated with gold and the morphological characteristics of the attached cells determined using SEM (FEI Quanta 450).

In order to investigate the proliferation of hBMSCs on the functionalized scaffolds, a Cell Counting Kit-8 assay (Dojindo Molecular Technologies, Inc. Japan) was used in this study. Briefly, hBMSCs were cultured on scaffolds at an initial density of 10^4 cells per scaffold for 1, 3 and 7 days. Then 360ul of culture medium and 40ul CCK-8 solution was added to each well at each time point and incubated at 37 ^oC for another 4h. An aliquot of 100ul was taken from each well and transferred to a fresh 96 well plate. The light absorbance of these samples was measured at 450 nm with a spectrophotometric microplate reader (Bio-Rad 680, USA). All the results were demonstrated as the optical density (OD) values minus the absorbance of blank wells.

2.6. Differentiation of hBMSCs cultured on the functionalized MBG scaffolds.

To assess the development of the osteoblastic phenotype of hBMSCs grown on various types of scaffolds, ALP activity was performed on day 7 and 14 after seeding 1×10^5 hBMSCs on each scaffold (n = 3). All the experiments were done in triplicate

in 24-well culture plates. At the predetermined time point, culture medium was decanted and cell layer washed gently three times with PBS followed by washing once in cold 50 mM Tris buffer, and then cells were lysed in 200μl 0.2% Triton X-100. Lysates were sonicated after being centrifuged at 14,000 rpm for 15 min at 4 ^{o}C. 50 μl supernatant was mixed with 150μl working solution according to the manufacturer's protocol (Beyotime). The conversion of p-nitrophenylphosphate into p-nitrophenol in the presence of ALP was determined by measuring the absorbance at 405 nm with a microplate reader (Bio-Rad 680, USA). The relative ALP activity was obtained as the changed OD values divided by the reaction time and the total protein content.

The expression levels of osteogenesis-related genes (runt-related transcription factor 2 (RUNX2), osteocalcin(OCN), bone sialoprotein (BSP), bone morphgenetic protein-2(BMP-2) and collagen type I (COL-1)) were measured using the qRT-PCR. The cells were seeded at a density of 2×10^4 cells per scaffold, cultured for 7 and 14 days and harvested using TRIzol Reagent (Invitrogen Pty Ltd., Australia) to extract the RNA. The obtained RNA was reverse transcribed into complementary DNA (cDNA) using RevertAid First Strand cDNA Synthesis Kit (Thermo) and the qRT-PCR analysis was performed on an ABI Prism 7300 Thermal Cycler (Applied Biosystems, Australia) using SYBR Green detection reagent. The relative expression of the genes of interest was normalized against the housekeeping gene GAPDH. All samples were assayed in triplicate and independent experiments were performed. The mean cycle threshold (Ct) value of each target gene was normalized against the Ct value of GAPDH. The relative expression was calculated using the following formula:

$2^{-(\text{normalized average Ct})} \times 100$.

2.7. Statistics

The data were collected from three separate experiments and expressed as means ± standard deviation. The one-way ANOVA and Student–Newman–Keuls post hoc tests were used to determine the level of significance and P values <0.05 were considered to be significant.

3 Results

3.1. Characterization of the functionalized MBG scaffolds.

Fig. 1 shows the representative SEM images of the MBG, SH-MBG and NH_2-MBG scaffolds. All scaffolds exhibited the interconnected macroporous structure with macropore size ranging from 300 to 500μm, and the surface of the pore walls was smooth. TEM images of the MBG, SH-MBG and NH_2-MBG scaffolds are shown in Fig. 2. Similar to the MBG scaffolds, the SH-MBG and NH_2-MBG scaffolds also had a well-ordered and uniform mesoporous channel structure in the inner of matrix, and the mesopore size was estimated to be 3-4 nm, suggesting that the functionalization did not change the mesoporous structure of the MBG scaffolds.

Fig. 3 shows N_2 adsorption-desorption isotherms of the MBG, SH-MBG and NH_2-MBG scaffolds together with the corresponding pore size distributions. The type IV isotherms for these scaffolds are typical of a mesoporous structure, and the type H1 hysteresis loops (Fig. 3A) in the mesoporous range are characteristic of cylindrical pores, in accordance with the p6mm mesoporous structure.[25] After the

functionalization of SH or NH_2 groups on the surface of MBG scaffolds, the specific surface areas of the scaffolds decreased from 272 to 206 and 190 m^2g^{-1}, respectively, and the pore volume decreased from 0.26 to 0.19 and 0.17 cm^3g^{-1}, respectively. The pore size distributions of the MBG, SH-MBG and NH_2-MBG scaffolds calculated from desorption branches using the BJH model were narrow, and peaked at 3-4nm (Fig. 3B).

Fig. 4 shows FTIR spectra of the MBG, SH-MBG and NH_2-MBG scaffolds. After the MBG scaffolds were functionalized with SH and NH_2 groups, vibration peaks can be observed at 2800-3050 cm^{-1} assigned to the stretching bands of C-H and C-C bonds. Furthermore, the stretching bands at 1400-1600 $cm^{-1}$and 2450-2550 cm^{-1} assigned to the N-H bonds for the NH_2-MBG scaffolds and the S-H bonds for the SH-MBG scaffolds, respectively. The results indicated that the SH and NH_2 groups have been functionalized on the MBG scaffolds. As shown in Fig. 5, the surface zeta potential for MBG, SH-MBG and NH_2-MBG scaffolds was 5.5±1.9, -10.1±2.6 and 30.6±1.8 mV, respectively.

TG analysis further confirmed the functionalization of the MBG scaffolds with SH and NH_2 groups (Fig. 6). For the MBG scaffolds, there was only a 1.7% weight loss between 50 and 800 ^oC, being mainly associated with the loss of water molecules (about 50-250 ^oC) adsorbed onto the surface of the scaffolds and the condensation of silanol groups (about 250-800 ^oC). For the SH-MBG and NH_2-MBG scaffolds, the TG curves showed different weight loss behavior compared to the MBG scaffolds. The SH-MBG and NH_2-MBG showed 3.7% and 5.1% weight loss between 250 ^oC and

550 ^{o}C except for the weight loss of water molecules between 50 and 250 ^{o}C, which were attributed to the decomposition of SH and NH_2 functional groups.

The MBG, SH-MBG and NH_2-MBG scaffolds had similar interconnected macropores, and the porosities of them were estimated to be in the range of 84-86% (Table 1) by using Archimeds' principle. The compressive strengths of the MBG, SH-MBG and NH_2-MBG scaffolds were estimated to be 68.5±11.4, 67.1±10.5 and 66.0±10.6 KPa, respectively (Table 1), which were similar to the previously reported pure MBG scaffolds and doped MBG scaffolds samples (~ 55 kPa).[26, 27]

3.2 Ion dissolution and apatite mineralization ability of the functionalized MBG scaffolds.

Fig. 7 shows SEM images and EDS analysis for the MBG, SH-MBG and NH_2-MBG scaffolds before and after soaking in SBF for 3 and 7 days. SEM analysis showed that before soaking in SBF, the surfaces of three types of scaffolds were smooth (Fig. 7 A1, B1 and C1). After soaking for 3 days, some spherical particles were deposited on the surface of these scaffolds due to the apatite mineralization in SBF. The morphologies of these mineralized spherical apatite particles showed no obvious difference among the MBG, SH-MBG and NH_2-MBG scaffolds (Fig. 7 A3, B3 and C3). After soaking for 7 days, more spherical particles were deposited on the surface of these scaffolds. In addition, the thicker apatite layers were deposited on the SH-MBG and NH_2-MBG scaffolds compared to the MBG scaffolds, suggesting that the bioactive kinetics of the SH-MBG and NH_2-MBG scaffolds were faster than the MBG scaffolds. After soaking in SBF for 3 days, EDS analysis showed the Ca/P ratio of the MBG, SH-MBG and

NH_2-MBG scaffolds was 1.17, 1.29 and 1.39, respectively (A4, B4 and C4 in Fig. 7). At day 7, there were obvious characteristic peaks for Ca and P elements on each EDS spectrum, and the Ca/P ratio of the MBG, SH-MBG and NH_2-MBG scaffolds was 1.40, 1.48 and 1.58, respectively (A7, 7 and C7 in Fig. 7), which were close to the Ca/P ratio of 1.67 for apatite, indicating the apatite mineralization on the surfaces of these scaffolds.

Fig. 8 shows wide-angle XRD patterns of the MBG, SH-MBG and NH_2-MBG scaffolds before and after soaking in SBF for 7 days. Similar to the MBG scaffolds, the SH-MBG and NH_2-MBG scaffolds had no diffraction peaks on the patterns except for a broad reflection at $2\theta=20\text{-}35^{o}$, which indicates the amorphous phase of the scaffolds. In comparison, XRD patterns of the scaffolds immersed for 7 days in SBF showed peaks that corresponded with HA, confirming the apatite formation of the scaffolds.

The concentrations of Si, Ca and P ions in SBF after soaking the MBG, SH-MBG and NH_2-MBG scaffolds for different periods are shown in Fig. 9. It can be seen that the concentration changes of Ca, Si and P ions for each type of scaffolds were similar. The Si concentrations increased with increasing soaking time, while both Ca and P concentrations increased at the early soaking stage, and then decreased after 1 day. On the other hand, the SH-MBG and NH_2-MBG scaffolds showed a little lower concentrations of Si, Ca and P ions at the same soaking time compared to the MBG scaffolds, which might be that the SH and NH_2 functionalization slightly decreased the ion release rates due to the barrier role of the SH and NH_2 functional groups on the

surfaces of the scaffolds.

3.3 Cell responses to the functionalized MBG scaffolds.

To investigate cell responses to the functionalized MBG scaffolds, hBMSCs were used in this study. The attachment and morphology of hBMSCs on different MBG scaffolds were observed by SEM (Fig. 10). After 7 days of culture, hBMSCs were attached to the surface of the pore walls presenting well-spread morphology on each type of scaffolds. However, more hBMSCs were observed on the SH-MBG and NH_2-MBG scaffolds than the MBG scaffolds. LDH activity can indicate the possible cell membrane damages resulted from the material cytotoxicity. Fig. 11A shows the LDH activity of hBMSCs cultured on the MBG, SH-MBG and NH_2-MBG scaffolds for 3 days. Fewer LDH activities were detected in the culture medium with the SH-MBG and NH_2-MBG scaffolds, suggesting higher cell viability and better biocompatibility for the SH-MBG and NH_2-MBG scaffolds. The proliferation of hBMSCs cultured on the MBG, SH-MBG and NH_2-MBG scaffolds for 1, 3 and 7 days was determined by CCK-8 proliferation assay. As shown in Fig. 11B, all scaffolds supported hBMSCs' proliferation, and the proliferation rate on the NH_2-MBG scaffolds was significantly higher than that on the MBG scaffolds at day 1, 3 and 7 ($P< 0.05$). However, only at day 7 the proliferation rate on the SH-MBG scaffolds was significantly higher than that on the MBG scaffolds.

ALP activity of hBMSCs cultured on the functionalized MBG scaffolds for 7 and 14 days are shown in Fig. 12. The SH-MBG and NH_2-MBG scaffolds exhibited a significant enhanced ALP activity compared to the MBG scaffolds ($P< 0.05$).

However, there were no significant differences in ALP activity of hBMSCs on the SH-MBG and NH_2-MBG scaffolds ($P > 0.05$). Cell differentiation of hBMSCs on the functionalized MBG scaffolds was further evaluated by osteogenic gene expression determined by the expressions of osteogenic markers RUNX2, OCN, BSP, BMP-2 and CoL-1 at 7 and 14 days (Fig. 13). The results showed that the surface functionalization with SH and NH_2 groups on the MBG scaffolds significantly enhanced the expression levels of osteogenic markers, i.e. stimulating osteogenic differentiation of hBMSCs on the scaffolds. Furthermore, the NH_2-MBG scaffolds exhibited the highest expression levels.

4. Discussion

In recent years, research topic on cell-surface interactions is great of interesting, especially in the area of biomaterial researches for therapeutics, diagnostics, and regenerative medicine.[15-17] Study on the effect of surface chemical modification on cellular behavior, such as cell adhesion, proliferation and differentiation, is critical to assess optimal surface functionalities and cell-surface interactions for tissue regeneration.[4, 16] In this study, we successfully fabricated 3D hierarchically porous MBG scaffolds, and functionalized them with chemical groups (SH and NH_2) by a post-grafting technique. The functionalized MBG scaffolds maintained the textural and microstructural characteristics of the MBG scaffolds. Furthermore, the SH-MBG and NH_2-MBG scaffolds still exhibited high specific surface area (206 and 190 m^2g^{-1}, respectively) and large pore volume (0.19 and 0.17 cm^3g^{-1}, respectively). These

scaffolds had a hierarchical pore structure with 300-500 μm of macropore size, 3-4 nm of mesopore size and 84-86 % of porosity (Fig. 2 and Table 1). In general, the hierarchical pore architecture and high porosity of the scaffolds are of great importance for bone regeneration. Pore sizes larger than 100 μm enable cell seeding, tissue ingrowths and vascularisation. Nanopores in the microporous (<2 nm) or mesoporous (2–50 nm) range allow for molecule transportation for any nutrition, waste removal and signaling, and promote adsorption of biological agents and cell adhesion.[28, 29] Therefore, the functionalized MBG scaffolds had desirable hierarchical pore structure for bone regeneration.

Apatite mineralization of bioactive materials plays an important role in the formation and maintenance of the tissue-biomaterials interface.[30] By modifying with different functional groups, the bioactivity of the biomaterials could be improved or controlled to some extent.[13] On the other hand, our previous study demonstrated that MBG materials had superior apatite-forming bioactivity compared to conventional bioactive glass due to their high surface area and mesoporous structure.[22] In this study, the results showed that a thick layer of apatite could be deposited on the surfaces of the SH-MBG and NH_2-MBG scaffolds after soaking in SBF for 7 days, as revealed by SEM, EDS and XRD analyses (Fig. 7 and Fig. 8). In addition, the releases of Ca, Si and P ions from the SH-MBG and NH_2-MBG scaffolds were similar to those from the MBG scaffolds (Fig. 9). However, the bioactive kinetics of the SH-MBG and NH_2-MBG scaffolds were a little faster than the MBG scaffolds, although the surface area and pore volume of the SH-MBG and NH_2-MBG scaffolds exhibited a little

decrease due to the functionalization of SH and NH_2 groups. This suggested that the presence of SH and NH_2 groups on the MBG scaffolds could be beneficial for enhancing the bioactivity, which was in concordance with previous reports on the functionalized materials with SH and NH_2 groups.[31, 32] Sun et al. demonstrated that the functionalized MBG with NH_2 groups could promote the formation of spherical apatite particles, and the bioactivity did not decrease with the decreasing surface area.[31] Colilla et al. found that amino-polysiloxane matrices containing both SH and NH_2 groups could improve the bioactivity of the functionalized bioactive hybrid materials.[32] They proposed that H^+ transferring from silanols (Si–OH) to NH_2 groups could result in zwitterions-like species ($Si–O^+$, H_3N^+) in the solution. These zwitterions-like species could produce mobile H^+ that associate/dissociate with the surface, generating electric conduction to the surface, and hence accelerated the nucleation and growth of apatite. The accepted mechanism for apatite formation on MBG scaffolds was that Si–OH groups were formed since the Si–O–Si linkage became broken in SBF; meanwhile, an exchange took place between Ca^{2+} in the glass and H^+ of the solution. Then supersaturated Ca^{2+} in the solution congregated onto the negatively charged Si–OH groups, inducing nucleation and growth of apatite.[33] On the other hand, the SH and NH_2 groups have much stronger electrostatic interaction ability than the Si–OH groups, which facilitates to serve as nucleation points for HA mineralization when soaked in SBF, which might further contribute the better bone-forming bioactivity of SH-MBG and NH_2-MBG scaffolds.

The cell/material interaction has been shown to exert considerable influence on

adhesion, motility, proliferation and differentiation of bone-forming cells, which are the important steps that occur before bone mineralization.[34, 35] Therefore, the adhesion, proliferation, ALP activity and osteogenic expression of hBMSCs cultured on the functionalized MBG scaffolds were systematically investigated in this study. First of all, potential toxic effect of the surface functionalization on biomaterials to the surrounding bone-forming cells is critical for clinical applications. By using photo-induced grafting modification method, Ma et al. introduced OH, COOH or amide ($CONH_2$) groups onto poly-l-lactic acid (PLLA) membrane surfaces, and they found that the cytocompatibility of the modified PLLA membranes with OH or $CONH_2$ groups was greatly improved compared to that of the original PLLA membrane, but the modified PLLA membrane with COOH groups had even worse cytocompatibility although it possessed a similar hydrophilicity.[36] In this study, LDH activity in the culture media released by the cells was used as an index of cytotoxicity and the results suggested that the SH-MBG and NH_2-MBG scaffolds had lower cytotoxicity and better biocompatibility than the MBG scaffolds. Studies demonstrated that mesoporous materials can cause cell apoptosis duo to their ability to generate reactive oxygen species (ROS),[37-39] but certain surface modifications with functional groups, such as NH_2 or SH groups, can reduce the cytotoxicity of silica mesoporous materials.[40, 41] Therefore, it is possible that the lower cytotoxicity of the functionalized MBG scaffolds was attributed to the inhibition of ROS generation due to the SH and NH_2 functionalization on the MBG scaffolds.

Besides their good biocompatibility, the SH-MBG and NH_2-MBG scaffolds also

enhanced hBMSCs' adhesion and proliferation capacity (Fig. 10 and 11). It is widely believed that surface-dependent differences can modulate focal cell adhesion formation and intracellular signaling cascades, ultimately leading to changes in initial adhesion and long-term cellular behavior.[42, 43] Keselowsky et al. showed that surface chemistry-induced changes in fibronectin conformation lead to alterations in binding of specific integrin adhesion receptors.[44, 45] In particular, $\alpha_5\beta_1$ exhibits binding specificity to the conformation of fibronectin created by adsorption on OH and NH_2 SAMs. By contrast, both $\alpha_5\beta_1$ and $\alpha_v\beta_3$ bind to COOH, while neither displays specificity for fibronectin conformations formed on CH_3. These differential integrin binding profiles modulate short-term changes in focal adhesion formation and activation of intracellular signaling pathways that subsequently lead to alterations in cell adhesion.[45] In this study, SEM analysis showed that hBMSCs on the SH-MBG and NH_2-MBG scaffolds presented spindle-shape morphology with many filopodia extensions, which also indicated that these SH or NH_2 functionalized MBG scaffolds were not deleterious to hBMSCs with respect to adhesion and spreading. Compared to the MBG scaffolds, the SH-MBG and NH_2-MBG scaffolds provided more compatible environment for cell proliferation as shown in CCK-8 assay. Arima et al. reported that functional groups on the substrate surface had an impact on cell adhesion behaviors, where NH_2 groups encouraged better adhesion of human umbilical vein endothelial cells (HUVECs) than OH and COOH groups.[46] Okada et al. demonstrated that L929 cells dramatically adhered on the NH_2-modified TiO_2/silicone composite surface, and the number of cells adhering on the composite sheet increased with the increase in the

NH_2 group density.[47] Additionally, cationic NH_2 groups have been shown to exert a positive effect on initial cell adhesion and growth.[48] Therefore, the SH-MBG and NH_2-MBG scaffolds could remarkably enhance cell adhesion and proliferation compared to the MBG scaffolds.

To date, a very few studies report on hBMSCs differentiated in vitro into osteogenic lineages without any exogenous soluble differentiation factor, exploiting predetermined surface functionalization. Interestingly, our results demonstrated that the SH-MBG and NH_2-MBG scaffolds promoted osteogenic differentiation as compared to the MBG scaffolds, which was indicated by the enhanced ALP activity and bone-related gene expression of hBMSCs (Fig. 12 and 13). Previous studies have shown that surface properties of the MBG materials can be seriously affected by modifying with functional groups, leading to the changes in bioactive behavior since it strongly depends on the ion exchange with the hydric environment.[10, 49] Moreover, high apatite-forming bioactivity promotes osteoblastic activity by absorbing serum proteins and growth factors to stimulate cell proliferation and differentiation.[50] Previously, the NH_2 and SH-modified surfaces were found to promote and maintain osteogenesis of hBMSCs both in the presence and absence of biological stimuli.[16, 51] Recently, COOH, OH, NH_2 groups and their combinations functionalized electrospun fibers were demonstrated to support HA formation on the fiber surfaces, which further stimulated MC3T3-E1 cells proliferation and osteogenic differentiation.[13] Curran et al. demonstrated that the increased levels of osteogenic markers observed when cells were cultured in contact with the NH_2 modified surfaces could be related to an

increase in vitronectin adsorption to the surface and subsequent focal contact formation and cell signaling.[48] Furthermore, integrin-specific interactions with fibronectin were proved to be essential for osteogenic differentiation, as incubation with β1-blocking antibodies inhibited differentiation by the MC3T3-E1 osteoblast-like cell line on NH_2 and OH surfaces.[51] Therefore, changing the surface chemistry could control the differentiation pathways of the MSCs. In this study, it might be presumed that the enhancement of osteogenesis mineralization of hBMSCs on the SH-MBG and NH_2-MBG scaffolds could be attributed to the synergistic effects of multiple factors, such as the positive influence of reactive functional groups on serum proteins and growth factors attachment/conformation, which further improved the HA nucleation, directed bone-forming cells anchorage and movement, and ultimately inducing signaling pathways that push the population down a long-term osteogenic pathway.[52] However, the in-depth mechanism that led to the enhanced hBMSCs adhesion, proliferation and osteogenic differentiation by the presently fabricated SH-MBG and NH_2-MBG scaffolds requires further investigation, and the bone generation capability of the functionalized MBG scaffolds would be further confirmed in animal experiments.

5. Conclusion

The functionalized MBG scaffolds with SH and NH_2 functional groups were successfully prepared by a post-grafting technique. The functionalized MBG scaffolds not only had hierarchical pore architecture (macropore of 300-500μm and mesopore

of 3-4nm) and high porosity (84-86%), but also possessed good apatite mineralization ability and biocompatibility. Importantly, the SH-MBG and NH_2-MBG scaffolds significantly enhanced hBMSCs' adhesion, proliferation and differentiation compared to the MBG scaffolds. This study suggested that the functionalization of MBG scaffolds with special functional groups is a viable way to tailor surface characteristics and bioactivity for stimulating biological responses of hBMSCs. Therefore, the functionalized MBG scaffolds are promising for their potential in bone regeneration applications.

Acknowledgements

The authors gratefully acknowledge the support by the Program for Professor of Special Appointment (Eastern Scholar) at Shanghai Institutions of Higher Learning, National Natural Science Foundation of China (No. 81371936 and 51302170,), Shanghai Nature Science Foundation (No.13ZR1458600) and Innovation Program of Shanghai Municipal Education Commission (No. 14YZ085).

Table 1. Structural parameters, porosity and compressive strength of MBG, SH-MBG and NH_2-MBG scaffolds

Samples	S_{BET} (m^2/g)	V_P (cm^3g^{-1})	R_P (nm)	Porosity (%)	compressive strength (KPa)
MBG	272	0.26	3.76	84.2±0.8	68.5±11.4
SH-MBG	206	0.19	3.76	85.5±0.4	67.1±10.5
NH_2-MBG	190	0.17	3.52	85.9±0.6	66.0±10.6

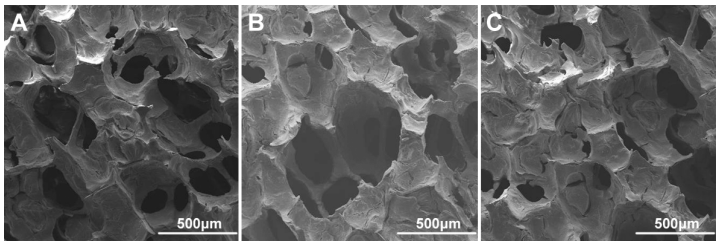

Fig. 1 SEM analysis for MBG (A), SH-MBG (B) and NH_2-MBG (C) scaffolds. Magnification: ×200 for A, B and C.

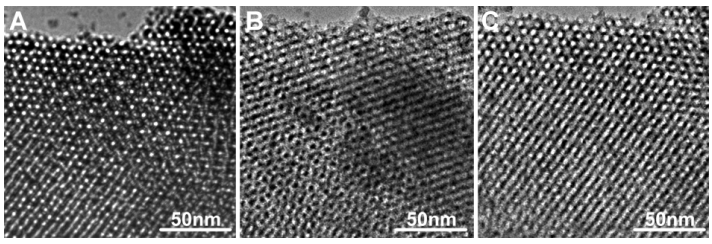

Fig. 2 TEM images of MBG (A), SH-MBG (B) and NH_2-MBG (C) scaffolds.

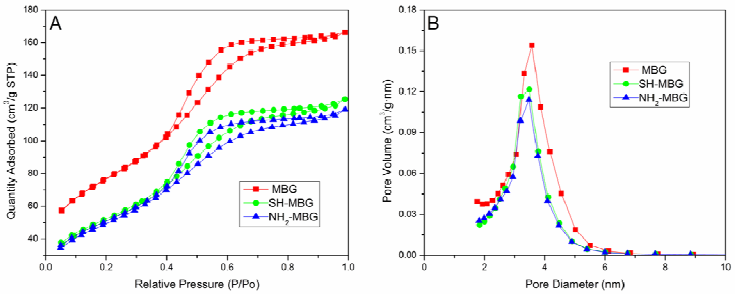

Fig. 3 (A) N_2 adsorption–desorption isotherms and (B) the corresponding pore size distributions of MBG, SH-MBG and NH_2-MBG scaffolds.

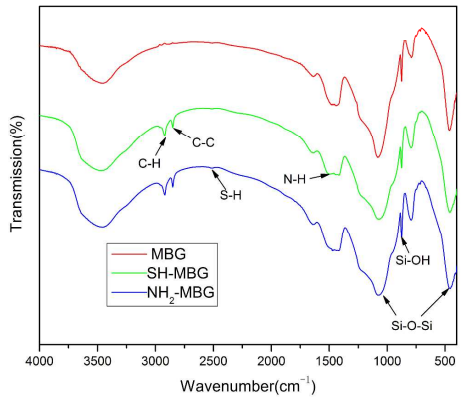

Fig. 4 FTIR analysis for MBG, SH-MBG and NH_2-MBG scaffolds.

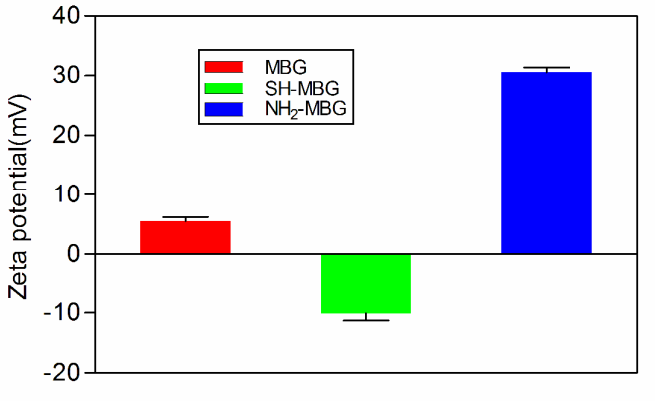

Fig. 5 The surface zeta potential data for MBG, SH-MBG and NH_2-MBG scaffolds.

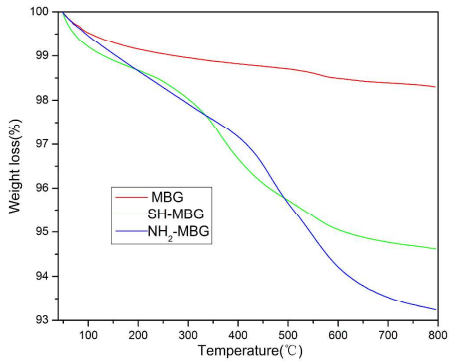

Fig. 6 TG analysis for MBG, SH-MBG and NH_2-MBG scaffolds.

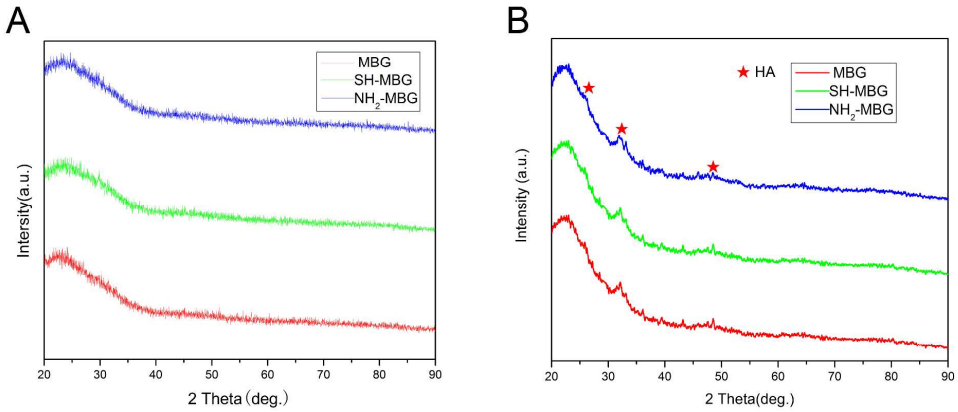

Fig. 7 Wide-angle XRD analysis for MBG, SH-MBG and NH_2-MBG scaffolds before and after soaking in SBF for 7 days.

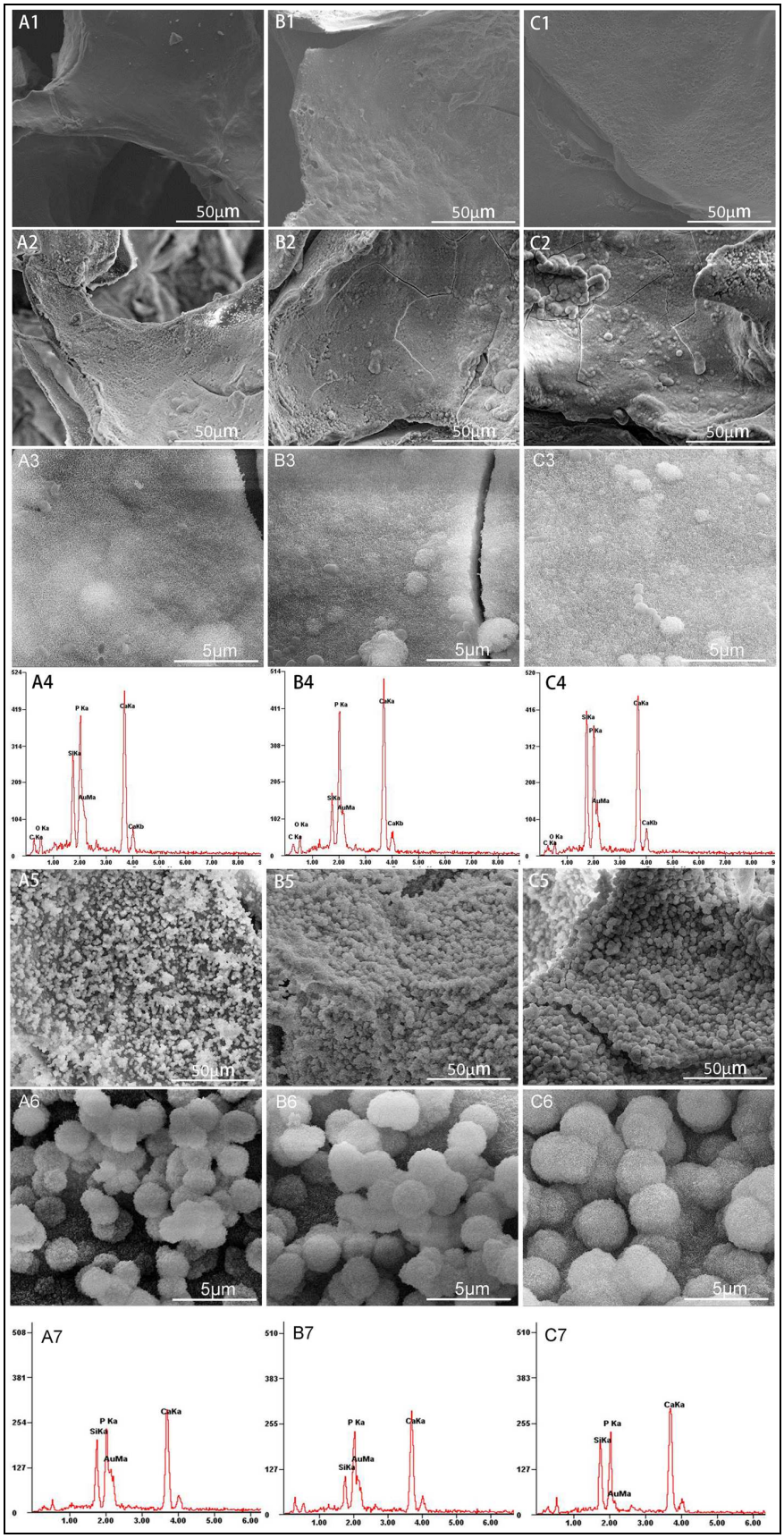

Fig. 8 SEM images for the MBG (A1), SH-MBG (B1) and NH_2-MBG (C1) scaffolds before soaking in SBF; SEM images for the MBG (A2, A3), SH-MBG (B2, B3) and NH_2-MBG (C2, C3) scaffolds after soaking in SBF for 3 days; SEM images for the MBG (A5, A6), SH-MBG (B5, B6) and NH_2-MBG (C5, C6) scaffolds after soaking in SBF for 7 days; EDS analysis for the MBG (A4), SH-MBG (B4) and NH_2-MBG (C4) scaffolds after soaking in SBF for 3 days. EDS analysis for the MBG (A7), SH-MBG (B7) and NH_2-MBG (C7) scaffolds after soaking in SBF for 7 days. Magnification: ×2000 for A1, B1, C1, A2, B2, C2, A5, B5, C5; ×20,000 for A3, B3, C3, A6, B6 and C6.

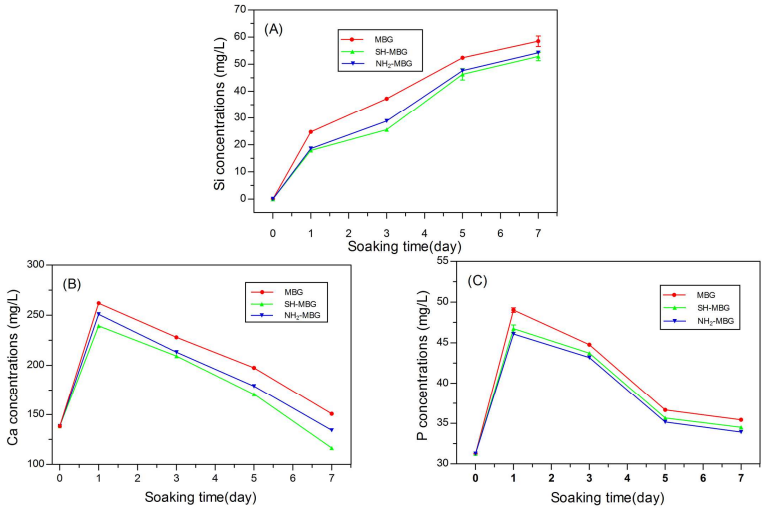

Fig. 9 Si (A), Ca (B) and P (C) ion concentrations in SBF solutions after soaking the MBG, SH-MBG and NH_2-MBG scaffolds for various time periods.

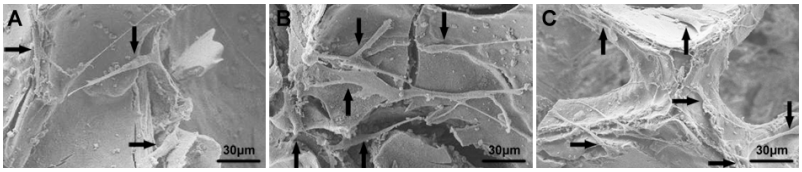

Fig. 10 SEM images of the attachment of hBMSCs cells on the MBG (A), SH-MBG (B) and NH_2-MBG (C) scaffolds after culturing for 7 days.

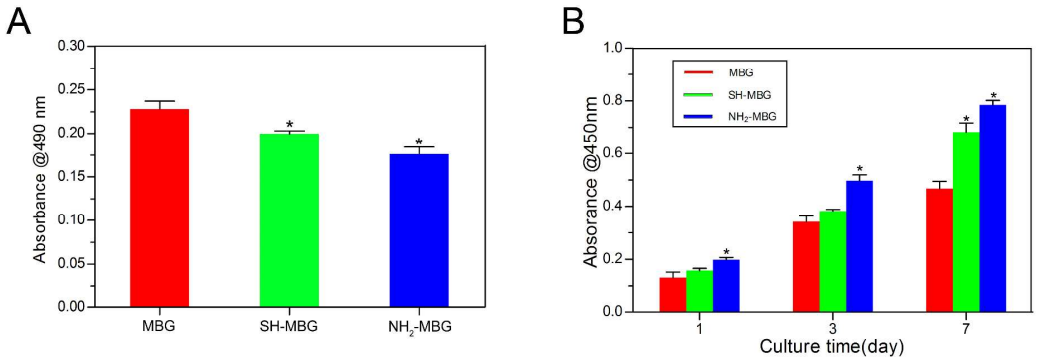

Fig. 11 (A) The LDH activity of hBMSCs cultured on the MBG, SH-MBG and NH_2-MBG scaffolds for 3 days. (B) The proliferation of hBMSCs cultured on the MBG, SH-MBG and NH_2-MBG scaffolds for 1, 3 and 7 days.

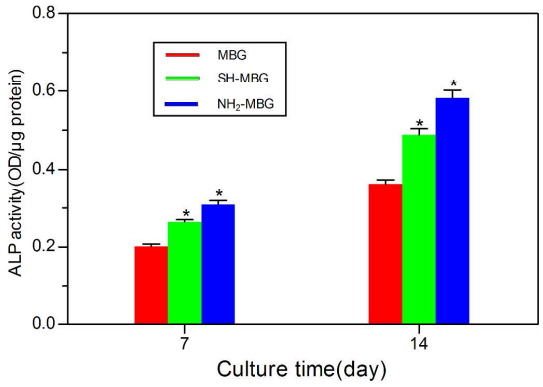

Fig. 12 The ALP activity of hBMSCs cultured on the MBG, SH-MBG and NH_2-MBG scaffolds for 7 and 14 days.

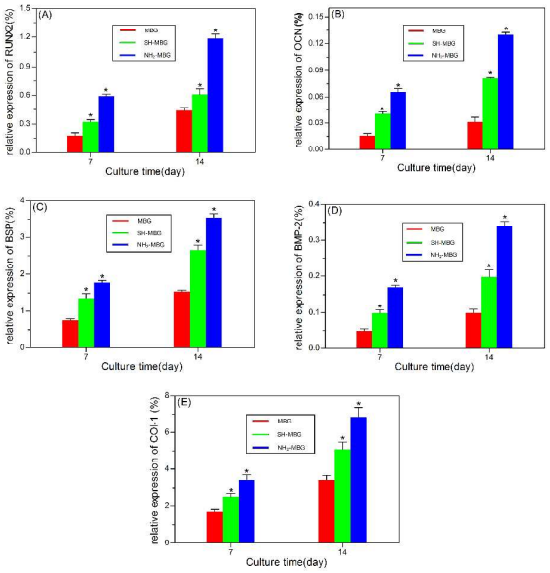

Fig. 13 Osteogenic gene expression of RUNX2 (A), OCN (B), BSP (C), BMP-2 (D) and COL-1 (E) for hBMSCs cultured on the MBG, SH-MBG and NH_2-MBG scaffolds analyzed by qRT-PCR for 7 and 14 days.

References

1. Y. Tabata, *Drug Discov. Today*, 2001, **6**, 483-487.
2. M. K. Nguyen, O. Jeon, M. D. Krebs, D. Schapira and E. Alsberg, *Biomaterials*, 2014, **35**, 6278-6286.
3. Z. Ma, M. Kotaki, R. Inai and S. Ramakrishna, *Tissue Eng.*, 2005, **11**, 101-109.
4. V. L. Lapointe, A. T. Fernandes, N. C. Bell, F. Stellacci and M. M. Stevens, *Advanced healthcare materials*, 2013, **2**, 1644-1650.
5. J. L. Charest, A. J. Garcia and W. P. King, *Biomaterials*, 2007, **28**, 2202-2210.
6. W. G. Brodbeck, G. Voskerician, N. P. Ziats, Y. Nakayama, T. Matsuda and J. M. Anderson, *J. Biomed. Mater. Res. A*, 2003, **64**, 320-329.
7. B. G. Keselowsky, L. Wang, Z. Schwartz, A. J. Garcia and B. D. Boyan, *J. Biomed. Mater. Res. A*, 2007, **80**, 700-710.
8. D. S. Benoit, M. P. Schwartz, A. R. Durney and K. S. Anseth, *Nature materials*, 2008, **7**, 816-823.
9. F. R. Maia, S. J. Bidarra, P. L. Granja and C. C. Barrias, *Acta Biomater.*, 2013, **9**, 8773-8789.
10. A. Lopez-Noriega, D. Arcos and M. Vallet-Regi, *Chemistry*, 2010, **16**, 10879-10886.
11. A. Nieto, M. Colilla, F. Balas and M. Vallet-Regi, *Langmuir*, 2010, **26**, 5038-5049.
12. M. Vallet-Regi, I. Izquierdo-Barba and M. Colilla, *Philosophical transactions. Series A, Mathematical, physical, and engineering sciences*, 2012, **370**, 1400-1421.
13. W. Cui, X. Li, C. Xie, H. Zhuang, S. Zhou and J. Weng, *Biomaterials*, 2010, **31**, 4620-4629.

14. G. K. Toworfe, R. J. Composto, I. M. Shapiro and P. Ducheyne, *Biomaterials*, 2006, **27**, 631-642.
15. A. El-Fiqi, J. H. Lee, E.-J. Lee and H.-W. Kim, *Acta Biomater.*, 2013, **9**, 9508-9521.
16. J. M. Curran, R. Chen and J. A. Hunt, *Biomaterials*, 2006, **27**, 4783-4793.
17. J. E. Phillips, T. A. Petrie, F. P. Creighton and A. J. Garcia, *Acta Biomater.*, 2010, **6**, 12-20.
18. F. Baino, S. Fiorilli, R. Mortera, B. Onida, E. Saino, L. Visai, E. Verne and C. Vitale-Brovarone, *Journal of applied biomaterials & functional materials*, 2012, **10**, 12-21.
19. C. Wu and J. Chang, *Interface focus*, 2012, **2**, 292-306.
20. C. Wu and J. Chang, *J. Control. Release*, 2014, DOI: 10.1016/j.jconrel.2014.04.026.
21. J. Zhang, S. Zhao, Y. Zhu, Y. Huang, M. Zhu, C. Tao and C. Zhang, *Acta Biomater.*, 2014, **10**, 2269-2281.
22. Y. Zhu, C. Wu, Y. Ramaswamy, E. Kockrick, P. Simon, S. Kaskel and H. Zrelqat, *Microporous Mesoporous Mater.*, 2008, **112**, 494-503.
23. T. Kokubo and H. Takadama, *Biomaterials*, 2006, **27**, 2907-2915.
24. T. Matsubara, K. Suardita, M. Ishii, M. Sugiyama, A. Igarashi, R. Oda, M. Nishimura, M. Saito, K. Nakagawa, K. Yamanaka, K. Miyazaki, M. Shimizu, U. K. Bhawal, K. Tsuji, K. Nakamura and Y. Kato, *J. Bone Miner. Res.*, 2005, **20**, 399-409.
25. W. Xia and J. Chang, *J. Control. Release*, 2006, **110**, 522-530.
26. C. Wu, Y. Zhou, C. Lin, J. Chang and Y. Xiao, *Acta Biomater.*, 2012, **8**, 3805-3815.
27. C. Wu, Y. Zhou, M. Xu, P. Han, L. Chen, J. Chang and Y. Xiao, *Biomaterials*, 2013, **34**, 422-433.
28. J. R. Jones and L. L. Hench, *J. Biomed. Mater. Res. B Appl. Biomater.*, 2004, **68**, 36-44.
29. A. Garcia, I. Izquierdo-Barba, M. Colilla, C. L. de Laorden and M. Vallet-Regi, *Acta Biomater.*, 2011, **7**, 1265-1273.
30. X. Liu, M. N. Rahaman, Y. Liu, B. S. Bal and L. F. Bonewald, *Acta Biomater.*, 2013, **9**, 7506-7517.
31. S. Jin, L. Yongsheng, L. Liang, Z. Wenru, L. Lei, G. Jianhua, R. Meiling and S. Jianlin, *J. Non-Cryst. Solids*, 2008, **354**, 3799-3805.
32. M. Colilla, A. J. Salinas and M. Vallet-Regi, *Chem. Mater.*, 2006, **18**, 5676-5683.
33. I. Izquierdo-Barba, A. J. Salinas and M. Vallet-Regi, *J. Biomed. Mater. Res.*, 1999, **47**, 243-250.
34. J. N. Beresford, S. E. Graves and C. A. Smoothy, *Am. J. Med. Genet.*, 1993, **45**, 163-178.
35. Y. Ramaswamy, C. Wu, H. Zhou and H. Zreiqat, *Acta Biomater.*, 2008, **4**, 1487-1497.
36. Z. Ma, C. Gao, Y. Gong and J. Shen, *Biomaterials*, 2003, **24**, 3725-3730.
37. B. Fubini and A. Hubbard, *Free Radic. Biol. Med.*, 2003, **34**, 1507-1516.
38. J. J. Wang, B. J. Sanderson and H. Wang, *Environ. Mol. Mutagen.*, 2007, **48**, 151-157.
39. E. Gazzano, F. Turci, E. Foresti, M. G. Putzu, E. Aldieri, F. Silvagno, I. G. Lesci, M. Tomatis, C. Riganti, C. Romano, B. Fubini, N. Roveri and D. Ghigo, *Chem. Res. Toxicol.*, 2007, **20**, 380-387.
40. A. J. Di Pasqua, K. K. Sharma, Y. L. Shi, B. B. Toms, W. Ouellette, J. C. Dabrowiak and T. Asefa, *J. Inorg. Biochem.*, 2008, **102**, 1416-1423.
41. Z. Tao, B. B. Toms, J. Goodisman and T. Asefa, *Chem. Res. Toxicol.*, 2009, **22**, 1869-1880.
42. E. K. Yim and K. W. Leong, *Nanomedicine*, 2005, **1**, 10-21.
43. R. G. Flemming, C. J. Murphy, G. A. Abrams, S. L. Goodman and P. F. Nealey, *Biomaterials*,

1999, **20**, 573-588.

44. B. G. Keselowsky, D. M. Collard and A. J. Garcia, *J. Biomed. Mater. Res. A*, 2003, **66**, 247-259.
45. B. G. Keselowsky, D. M. Collard and A. J. Garcia, *Biomaterials*, 2004, **25**, 5947-5954.
46. Y. Arima and H. Iwata, *Biomaterials*, 2007, **28**, 3074-3082.
47. M. Okada, S. Yasuda, T. Kimura, M. Iwasaki, S. Ito, A. Kishida and T. Furuzono, *J. Biomed. Mater. Res. A*, 2006, **76**, 95-101.
48. J. M. Curran, R. Chen and J. A. Hunt, *Biomaterials*, 2005, **26**, 7057-7067.
49. L. Kam, W. Shain, J. N. Turner and R. Bizios, *Biomaterials*, 2002, **23**, 511-515.
50. C. Loty, J. M. Sautier, H. Boulekbache, T. Kokubo, H. M. Kim and N. Forest, *J. Biomed. Mater. Res.*, 2000, **49**, 423-434.
51. B. G. Keselowsky, D. M. Collard and A. J. Garcia, *Proc. Natl. Acad. Sci. U. S. A.*, 2005, **102**, 5953-5957.
52. H.-S. Yu, S.-J. Hong and H.-W. Kim, *Mater. Chem. Phys.*, 2009, **113**, 873-877.